Published in final edited form as:
Acta Neuropathol. 2013 September ; 126(3): . doi:10.1007/s00401-013-1145-2.

Interstitial fluid drainage is impaired in ischemic stroke and Alzheimer's disease mouse models

Michal Arbel-Ornath[1], **Eloise Hudry**[1], **Katharina Eikermann-Haerter**[2], **Steven Hou**[1], **Julia L. Gregory**[1], **Lingzhi Zhao**[1], **Rebecca A. Betensky**[3], **Matthew P. Frosch**[1,4], **Steven M. Greenberg**[1], and **Brian J. Bacskai**[1]

[1]Alzheimer Research Unit, Department of Neurology, Massachusetts General Hospital and Harvard Medical School, 114, 16th st., Charlestown, MA 02129, USA

[2]Stroke and Neurovascular Regulation Laboratory, Department of Radiology, Massachusetts General Hospital and Harvard Medical School, 149, 13th st., Charlestown, MA 02129, USA

[3]Department of Biostatistics, Harvard School of Public Health, 50 Staniford Street, Boston, MA, USA

[4]C.S. Kubik Laboratory for Neuropathology, Department of Pathology, Massachusetts General Hospital and Harvard Medical School, 114, 16th st., Charlestown, MA 02129, USA

Abstract

The interstitial fluid (ISF) drainage pathway has been hypothesized to underlie the clearance of solutes and metabolites from the brain. Previous work has implicated the perivascular spaces along arteries as the likely route for ISF clearance, however it has never been demonstrated directly. The accumulation of amyloid β (Aβ) peptides in brain parenchyma is one of the pathological hallmarks of Alzheimer disease (AD), and it is likely related to an imbalance between production and clearance of the peptide. Aβ drainage along perivascular spaces has been postulated to be one of the mechanisms that mediates the peptide clearance from the brain. We therefore devised a novel method to visualize solute clearance in real time in the living mouse brain using laser guided bolus dye injections and multiphoton imaging. This methodology allows high spatial and temporal resolution and revealed the kinetics of ISF clearance. We found that the ISF drains along perivascular spaces of arteries and capillaries but not veins, and its clearance exhibits a bi-exponential profile. ISF drainage requires a functional vasculature, as solute clearance decreased when perfusion was impaired. In addition, reduced solute clearance was observed in transgenic mice with significant vascular amyloid deposition; we suggest the existence of a feed-forward mechanism, by which amyloid deposition promotes further amyloid deposition. This important finding provides a mechanistic link between cerebrovascular disease and Alzheimer disease and suggests that facilitation of Aβ clearance along the perivascular pathway should be considered as a new target for therapeutic approaches to AD and CAA.

Keywords

Alzheimer's disease; Amyloid β; Cerebral amyloid angiopathy; Interstitial fluids; Ischemic stroke; Perivascular space

Corresponding author: Brian Bacskai, Ph.D, Alzheimer Research Unit, Department of Neurology, Massachusetts General Hospital and Harvard Medical School, 114, 16th st. Charlestown, MA 02129, USA, Tel: 617-724-5306, bbacskai@partners.org.

Introduction

The brain extracellular fluids consist of blood, cerebrospinal fluid (CSF) and interstitial fluid (ISF). More is known about the CSF than the ISF with respect to its generation, composition, flow rates and paths. The ISF is thought to derive from metabolic activity of the tissue and capillary secretion of fluids and metabolites, along with some recycled CSF. Over a century of hypotheses and experiments have focused on the nature of the ISF, its origin, its relationship with the CSF and its dynamics (reviewed in [1]), however these efforts mainly used indirect measures and relied on postmortem analyses.

ISF drainage is not only an important aspect of normal brain function, but is also implicated in disease, particularly the two major brain amyloid β (Aβ) amyloidoses, Alzheimer's disease (AD) and cerebral amyloid angiopathy (CAA). As Aβ peptides are generated and cleared continuously in the brain, an imbalance between these two processes likely underlies this peptide's accumulation and deposition. Late onset sporadic AD in particular, which accounts for the vast majority of cases, is thought to be associated with failure to clear the peptide from the aging brain [10,33]. Several mechanisms mediating Aβ clearance from the brain have been described, including enzymatic degradation [20], transcytosis across the blood-brain barrier via the low-density lipoprotein receptor [3], microglia and perivascular macrophage uptake [12] and perivascular drainage along with the ISF [45]. The contribution of perivascular drainage of Aβ to cerebral Aβ levels raises the possibility that vascular pathologies may interfere with this process and thus affect the disease onset and progression. Using intracerebral dye injection and post mortem examination, altered perivascular drainage of dextran was correlated with both increase in age and CAA [16]. Additionally, we have previously shown that experimental vascular occlusion or stroke in an Aβ-expressing transgenic mouse model caused transient increases in amyloid accumulation [13].

Most prior studies of ISF drainage have utilized intracranial injections of soluble tracers and timed sacrifice of the animal, followed by anatomical mapping of the tracer spread. Intraparenchymal injection of soluble tracers, such as radioactive material, horseradish peroxidase, Evans blue, and India ink into different sites within rabbit and rat brains revealed a similar spread along the walls of cerebral arteries and eventual accumulation in the neck lymph nodes [4,7,39]. Although these past studies have contributed enormously to our understanding of ISF flow, they have been unable to define the dynamic nature of the ISF, the pathways by which it flows, and the driving forces that influence clearance rates. The major limitation of the prior approaches is that they monitor ISF flow in single postmortem snapshots rather than in real time in living animals.

In order to gain more quantitative information about the ISF flow with high spatial and temporal resolution, and to study the contribution of vascular function as well as amyloid deposition, we devised novel methods to visualize ISF drainage in the living mouse brain using multiphoton microscopy. To that end, we combined a craniotomy and laser-guided micropipette injection of fluorescent tracers into the brain parenchyma. This technique allowed us for the first time to watch ISF drainage in real time in mouse models of neurological disease. Our results indicate specific clearance of ISF by bulk flow along pericapillary and periarterial spaces and marked sensitivity of this process to an experimental model of stroke and to Aβ deposition.

Materials and Methods

Animals

C57BL/6J males, 3–6 months of age, were obtained from Charles River Laboratories. Myh11-cre,-EGFP mice, expressing EGFP in their smooth muscle cells, were obtained from

Jackson Laboratory (stock number 007742) and used at 6–12 months of age. APPswe:PS1dE9 mice, expressing the familial Swedish mutation in human amyloid precursor protein (APP) encoding gene and the exon 9 deletion variant of human presenilin 1 (PS1) gene both in the same locus under the control of PrP promoter [21], were obtained from Jackson Laboratory (stock number 00462). Mice of both genders were used at either at 6–8 months of age or at 2.5–3 months of age (pre-amyloid deposition). In each genotype, mice were equally distributed according to their gender. All studies were performed with the approval of the Massachusetts General Hospital Animal Care and Use Committee and in compliance with the National Institute of Health guidelines for the use of experimental animals.

Cranial window surgery

Mice were anesthetized with isoflurane (1.5% with pure O_2) and a cranial window, 6 mm in diameter, was implanted as previously described [36] with minor modifications. As this procedure is followed by laser guided pressurized micropipette injection, we did not use a coverglass to close the exposed brain area. Instead, a wax ring, made of warm paraffin, was placed around the exposed brain and agarose (1.5% in PBS) was applied to the brain surface to minimize movement artifacts (due to breathing and heart beat). PBS pH 7.4 was maintained above the agarose to keep the brain moist and enable imaging through a water immersion objective. Texas-red labeled dextran (70 kDa, 250μl of 12.5 mg/ml in sterile PBS, Life technologies) was injected into a lateral tail vein to provide a fluorescent angiogram.

In vivo imaging and pressure injections of fluorescent dextrans

For in-vivo imaging, an Olympus FluoView FV1000MPE multiphoton laser-scanning system mounted on an Olympus BX61WI microscope and an Olympus 25x dipping objective (NA=1.05) were used. A DeepSee Mai Tai Ti:sapphire mode-locked laser (Mai Tai; Spectra-Physics) generated two-photon excitation at 750 nm, and detectors containing three photomultiplier tubes (Hamamatsu, Ichinocho, Japan) collected emitted light in the range of 420–460, 495–540, and 575–630 nm. Mice were placed on the microscope stage and heated throughout the pipette injection and imaging session, using a heating pad with a feedback regulation from a rectal temperature probe (Harvard apparatus). Mouse anesthesia was maintained at 1–1.2% isoflurane. A patch pipette with a tip diameter of 2–3 μm was back-filled with 3μl of Cascade Blue labeled dextran (3kDa, 2mg/ml in sterile PBS; Life technologies) and inserted into the cortex to a depth of 100–150 μm from the surface using the visual guidance of Texas-red labeled brain vasculature. Once the micropipette was placed, a z-series (508μm × 508μm, 5μm steps, depth of about 200μm, 512 × 512 pixels) was taken before the injection. The dextran was then pressure-ejected under laser guidance from the pipette at 5–20 PSI for 10–30 seconds using the Picospritzer 2000 (AM Systems, Carlsborg, WA) and the same cortical volume was imaged with 2 min time lapse imaging for 30–45 min.

In the case of B6C3-APP/PS1 transgenic mice, a permanent catheter was attached to the tail vein prior to the imaging and used for injection of the BBB permeable derivative of Congo Red that binds fibrillar amyloid deposits, methoxy-XO4 (3.5 mg/Kg)[25], at the end of the session to visualize the Aβ aggregates on the vessel wall as well as in the parenchyma. Images of the same volume with the methoxy-XO4 positive stain were taken 30 min after the intravenous injection of the dye using the same acquisition and laser power parameters in all tested mice to allow comparison of amyloid burden across brains.

Transient hypertension

To characterize the effect of intra-peritoneal injection of phenylephrine (referred as PE in the text) on blood pressure, C57BL/6J males at 3–6 months of age were used (n=3). For full systemic physiological monitoring, the left femoral artery was catheterized for blood sampling and measurement of mean arterial pressure (MAP; ETH 400 transducer amplifier) under isoflurane anesthesia (2.5% induction, 1% maintenance, in O_2). Arterial blood gases and pH were measured once every 30 min during each experiment in 25 μl samples (Corning 178 blood gas/pH analyzer, Ciba Corning Diag). Mice were injected with 3mg/Kg PE (in PBS, pH 7.4; Baxter Healthcare Corporation) and mean arterial pressure (MAP) was monitored for 1 hr.

To evaluate the effect of increased peripheral blood pressure on perivascular drainage in the brain, we used a different cohort of C57BL/6J males and performed two consecutive pressure micropipette injections of Cascade Blue dextran. After the first time course, we injected through the peritoneum either PE (3mg/ Kg in PBS pH7.4, n=6) or an equal volume of PBS (n=7). 10 min later, the second pipette injection was performed followed by time lapse imaging with 2 min intervals.

Microstroke production

C57BL/6J males (n=6), 3–6 months of age, were used to evaluate the effects of microstroke on ISF drainage. To that end, the cranial window and micropipette injection were performed as described above. After the first injection and time lapse imaging, a focal stroke was induced via photothrombosis of Rose Bengal (Rose Bengal sodium salt, Sigma-Aldrich, USA). Rose Bengal was administered through a permanent intravenous catheter (100ul, 16.6mg/Kg in sterile PBS pH 7.4) as previously described [51] and immediately activated with a 543nm HeNe laser (at maximal power) directed at the selected arterial segment (~20 μm × 20 μm) for 2–3 min. Segments were selected from vessels with a diameter range of 20–50μm. RBC velocity was assessed before and after microstroke using bi-directional line scans along the length of the center of the vessels for the chosen vessel segments as well as other non-stroked segments, as previously described [24]. The resulting line scan (LS) image appears as streaks which represent non fluorescent RBC that move through a fluorescent background. The calculated slopes of these streaks are inversely proportional to the RBC velocity. After assuring that a microstroke was indeed induced a second pressure injection of the Cascade Blue dextran was performed (using identical parameters) and the same cortical volume was imaged at 2 min intervals for an additional 30 min.

Image processing and analysis

Image processing and analysis was performed using ImageJ software (http://rsbweb.nih.gov/ij/). Otherwise, to reduce noise, a median filter with radius 2 was applied to all volumes. To evaluate dextran clearance rates, regions of interest showing dye localization along vessel walls were selected manually from the individual 5μm slices, using the polygon selection tool. Dye intensity, measured in these regions of interest throughout the time course, was normalized to time zero. Curve fitting was done in MATLAB using the curve fitting tool box. We analyzed several summary measures that were independent of curve fitting, that reflect the rate of dye clearance along perivascular spaces including, time to 50% clearance, time to 75% clearance, area under the curve (AUC) at 30 minutes and area under the curve at 12 minutes (representing mostly the fast decay phase). We report results based on the measure of area under the curve (AUC) of the intensity vs. time plots up to 30 min as it includes the entire data set obtained throughout the imaging session without the need for curve fitting. Measurements of time to 50% and time to 75% of initial dye intensity followed similar qualitative trends to that of AUC measurement across the different experimental groups. Thus, for the sake of simplicity, we chose to report only the AUC measurements.

Area under the curve was measured using GraphPad Prism 5 software. Red blood cell (RBC) velocity was calculated from the repeated line scans as it is inversely proportional to the slope of the RBC streaks. A macro was written in Image J to detect the lines, calculate the slopes and invert the values to give the velocity. Vessel diameter was measured in Image J at three different points along the chosen vessel segment and averaged for each vessel. Arteries and veins were identified in the field of view according to their morphology and blood flow directionality. For illustration purposes, the maximal projection images of the EGFP mice were processed to remove autofluorescence lipofuscin particles.

Statistical analyses

To compare groups based on AUC, we tested the hypotheses of interest within the framework of a mixed effects model that included a random effect for mouse to adjust for correlation within mouse, and fixed effects for the comparison of interest (e.g., pre versus post or vessel type), and in some cases for vessel diameter. Examination of residuals from the fitted model supported the assumptions of linearity and normality. For sensitivity analysis, we also tested our hypotheses using an extension of the Wilcoxon nonparametric, rank-based test to clustered data structures [9]. The qualitative results from these analyses support those from the parametric linear mixed effects models.

Results

Visualizing ISF drainage along perivascular spaces

To visualize ISF flow in the living mouse brain in real time, we combined laser guided bolus injections of fluorescent tracers and multiphoton time lapse imaging of cortical volumes. The tracer was Cascade Blue conjugated to 3kDa dextran which has a molecular weight similar to that of monomeric Aβ. Intravenous injection of 70kDa dextran conjugated to Texas Red was used to label the brain vasculature and allowed insertion of the pipette with minimal damage to the surrounding blood vessels.

Immediately (as soon as 2 min) after the bolus injection of dextran, dye was evident throughout the parenchyma but appeared to be concentrated along the external contours of vessels within the injection volume, in a location consistent with the vascular basement membrane (Fig. 1a and b). Dextran alignment along the vessel wall was restricted to arteries and capillaries, suggesting these as the route for ISF drainage. To increase our understanding of dye localization within the perivascular space and the basement membrane of the vessel we performed dextran injections in the Myh11-cre,-EGFP mice which express EGFP in smooth muscle cells (Fig. 2). Similar to our previous observations, in these mice dextran accumulated rapidly along the vessel wall. While most of the dye was detected in the perivascular space/ perivascular parenchyma, some dye, at lower intensities, was evident within the basement membrane between the smooth muscle cells (Fig. 2b, yellow arrows). On very rare occasions we could detect the dextran inside the smooth muscle cells, suggesting minimal dye loading by these cells. Time lapse imaging and quantification of the perivascular dye burden revealed that the ISF drainage followed a bi-exponential mode of decay (Fig1c); this is more consistent with bulk flow than with diffusion as the underlying clearance mechanism. Dye clearance from the parenchyma also followed a bi-exponential mode of decay, though much faster compared with dye along the vessel wall, presumably because of the contribution of multiple perivascular pathways (ROI 5, Fig. 1b and c). We controlled for the contribution of dye bleaching during the imaging session to the measured outcome by focusing on the pipette tip above the surface of the brain and quantifying the change in dye intensity throughout a period of 30 min (Figure 1d, light blue linear curve). A small degree of variability was observed for dye clearance around different vessel segments within a brain as well as across brains (Fig. 1c and d). As a summary measure for each curve

we calculated the area under the curve (AUC) of the intensity vs. time plots up to 30 min as it includes the entire data set obtained throughout the imaging session without the need for curve fitting. As reflected by AUC measures, ISF drainage did not depend on vessel diameter in the healthy brain (Fig. 1e, mean increase per unit diameter 0.005 ±0.029, p=0.861).

Transient systemic hypertension does not affect ISF drainage

Having observed selective dye localization to arteries rather than veins, we hypothesized that arterial pulse pressures may play a major role in driving the process and thus may account for the fast decay observed. Thus, we explored whether an increases in systemic blood pressure could enhance ISF drainage. The impact of systemic blood pressure on cerebral blood flow (CBF) is substantially limited, however, by the autoregulation process in which arterial diameters change in response to blood pressure or perfusion pressure variations to maintain constant CBF [31]. To evaluate the effect of modest change in blood pressure on ISF drainage, we used phenylephrine (PE), a selective α1-adrenergic receptor agonist, and measured ISF drainage in two consecutive bolus dye injections before and after PE administration. The administration of PE induced an increase in the mean arterial pressure (MAP, measured via a femoral artery catheter) as soon as 2 min after injection, reaching a plateau within 8–10 min after injection with an average amplitude of 25.5 ± 4.4 % increase of the initial MAP and persisting up to 1 hour after injection. In a separate cohort of mice we tested the effect of PE on ISF drainage by administering either the compound (n=6) or equivalent volume of PBS (n=7) i.p between the two bolus dye injections. Transient systemic hypertension did not affect the drainage of ISF along perivascular spaces as evident in figure 2 (AUC 1^{st} inj. vs. 2^{nd} inj: PE: p=0.88, control: p=0.705). The absence of a change after PE administration suggests either that the CBF autoregulation is effective in this range of pressure changes, or that mean arterial pressure plays a small role in the rate of ISF clearance along the perivascular drainage pathway.

Ischemic stroke impairs ISF drainage

Considering the mild effect of systemic hypertension on ISF drainage we set out to explore the effect of more dramatic manipulations to the brain vasculature including focal ischemic stroke and Alzheimer's disease. Epidemiological studies have shown a strong association between vascular factors predisposing to cerebrovascular disease, stroke and AD [17,23,26]. We have recently shown that focal stroke can trigger accelerated amyloid deposition in mouse models of AD without changes in the levels of key players in the amyloid cascade including APP, BACE1, presenilin 1, neprilysin and Insulin degrading enzyme (IDE) [13]. We therefore hypothesized that Aβ clearance along perivascular spaces may be impaired after stroke.

To study the immediate effects of stroke in real time, we focally disrupted vascular perfusion using the photosensitizing agent, Rose Bengal, paired with irradiation of individual vessel segment [43,51]. Parenchymal dye injections followed by time lapse imaging were performed before and after photo-occlusion of a single vessel in order to determine the impact of altered luminal flow on clearance in the perivascular space. To verify that the laser irradiation of Rose Bengal indeed led to a cessation of blood flow in the desired vessel, we measured the instantaneous velocity of red blood cells before and after the irradiation, using line scans (LS) along the vessel length. Maximum intensity projection images of the brain vasculature and the intraluminal line scans before and after the focal stroke (occlusion, red box) show cessation of the blood flow in the occluded vessel (Fig. 4a and 4b, Ls1). The RBC velocity in a non-occluded vessel in the same field (Ls2) was not appreciably affected by the focal occlusion. Dye localization along the vessel wall was quantified for both the occluded and non-occluded vessels before and after the single vessel

occlusion (pre and post, respectively) and showed an obvious impairment in dye clearance along the perivascular space of the occluded vessel with no effect on the non-occluded vessel (Fig. 4c and d). AUC measured on the first injection (i.e. before vessel occlusion) were not different between subsequently occluded, non-occluded and vessels from untreated brains (occluded vs. non occluded p=0.753; non-occluded vs. vessels from untreated brains p=0.899). AUC, calculated for all vessels from all experiments before and after occlusion, was significantly increased in the occluded vessels after induction of stroke with minimal change in the non-occluded vessels from the same brains, as well as in vessels from untreated brains (Fig. 4e). These findings indicate a marked impairment of clearance along occluded vessels (p-values for before vs. after comparison: 0.001 for occluded vessels, 0.243 for non-occluded vessels, 0.705 for vessels from untreated mice). The majority of occluded vessels no longer decayed in a bi-exponential fashion or reached the 50% decay of initial dye intensity within the 30 min of imaging. These results demonstrate that ISF clearance is driven by arterial blood flow, and that an ischemic stroke can markedly reduce the efficiency of solute clearance by this pathway.

Amyloid deposition impairs ISF drainage

Amyloid deposition in the walls of small cerebral arteries and capillaries (CAA) occurs in over 80% of AD patients as well as 10–40% of the elderly population without AD [2,15]. To investigate the effect of amyloid deposition on ISF drainage along perivascular spaces, we imaged and quantified ISF drainage in APPswe/PS1dE9 (APP/PS1) transgenic mice and their wild type littermates. These mice develop parenchymal amyloid deposits and CAA, starting at 4–5 months of age with a progressive increase up to 12 months of age [14]. Transgenic mice and their wild type littermates were tested at 6–8 months of age (n=8 for each genotype), when both CAA and plaque deposition are well established. Young (pre-deposition) transgenic mice (2.5–3 months of age, n=5) were used for comparison. In each genotype, we included mice of both genders as we have previously reported that CAA progression rates were independent of gender in both the Tg2576 [32] and the APP/PS1 mice [14]. We were able to follow dye accumulation along vessel walls in both transgenic and wild type brains immediately after the dextran bolus injection (Fig. 5a, b for tg and 5d, e for wt littermates). Comparison of decay parameters between the young C57BL/6J mice used for the PE and stroke studies and wild type B6C3 mice (APP/PS1 littermates), used for this study at 6–8 months of age, showed no difference in ISF drainage (AUC: C57BL/6J–13.02 ± 1.22; B6C3–13.73 ± 1.01, p=0.659), ruling out the possibility age-dependent vascular effect on the process at this age. Plaque and CAA bearing transgenic mice showed impaired ISF drainage as reflected by 60% increase in the AUC (Fig. 5g, transgenic vs. wild-type p=0.007). Conversely, young transgenic mice without plaques or CAA showed clearance properties similar to that of the wild type littermates and significantly different from that of the plaque- and CAA-bearing mice (tg vs. young-tg p=0.011; wt vs. young tg p=0.855), demonstrating that amyloid deposition has a profound effect on ISF clearance that may further exacerbate the progression of disease.

Discussion

We have developed a novel methodology to visualize ISF drainage along perivascular spaces in real time in the living mouse brain. Fluorescent-labeled dextran injection into the brain parenchyma resulted in fast movement of the dye towards cerebral arteries and capillaries (but not veins) and subsequent clearance along perivascular spaces. The fluorescent dye accumulated along the vessel wall, occupying the perivascular space and/or perivascular parenchyma, and could be observed at lower intensities within the basement membrane between the smooth muscle cells. In the healthy mouse brain, ISF drainage occurred with a bi-exponential mode of decay that was similar among cortical vessels in the

same brain as well as across brains and was independent of vessel diameter. Transient systemic hypertension within a range in which brain autoregulation is effective [31] did not affect this process. Conversely, focal occlusion of a single vessel segment dramatically impaired ISF drainage along this vessel with minimal effect on other vessels in the field of view. Transgenic mouse models of Alzheimer's disease demonstrated impairment in ISF drainage along perivascular spaces in mice with amyloid deposits but not in young mice prior to the onset of amyloid deposition.

Over the past century, many studies have revealed conflicting data as to the existence of ISF drainage, the pathways by which it flows, and the nature of its sources. Although the perivascular space was once thought to be open only to the subarachnoid space and closed to the brain parenchyma [48] [44], it has been confirmed since that tracers injected into the parenchyma spread inward from the brain along perivascular spaces of arteries [50]. Quantitative efforts combining histological and mathematical modeling showed that tracer distribution after infusion into the rat brain parenchyma exceeded the one predicted by diffusion equation in terms of both concentration of the tracer and the distance it traveled [27], supporting a contribution from ISF flow along perivascular spaces. In support of these findings, injecting tracers of different molecular weights into the brain parenchyma showed similar rates of clearance [1,6], also arguing in favor of bulk flow rather than diffusion as a major component of ISF flow. These studies and others (for review see [1]) used injections of labeled tracers and qualitative post mortem evaluation of their distribution in the brain. To be able to appreciate ISF drainage as a dynamic process, we designed and executed a method to observe this process in real time in the intact mouse brain. The data obtained here show rapid dye accumulation along the basement membrane of arteries and capillaries, excluding veins, consistent with previous reports[6]. The observed bi-exponential mode of decay of the tracer along these spaces argues in favor of bulk flow as a major component controlling this process rather than diffusion alone [29]. The exclusive drainage of ISF along arterial perivascular spaces suggest that arterial pulsation may drive the fast component of the observed bi-modal decay, with diffusion potentially accounting for the slow decay. We did not, however, see major differences in clearance rates of 3kDa and 70kDa dextrans (data not shown), arguing against diffusion as a major contributor for this process. In the same control experiments, a 2000 kDa dextran did not exhibit clearance from the brain parenchyma, consistent with a physical size limit for diffusion in the extracellular space [18].

The dramatic impairment of ISF drainage we observed after focal vessel occlusion strengthens the contribution of cerebral perfusion as a major driving force of this process. Acute BBB breakdown and leakage of plasma proteins following a thrombotic event were previously reported [11,34] and may account for an additional plausible mechanism for impaired ISF clearance along perivascular spaces. Changes in BBB permeability has been observed in early stages of AD [47]. As such, serum proteins, including albumin and immunoglobulin were shown to be highly concentrated in cortical areas with dense plaque pathology. These data suggest that alterations in BBB permeability manifested chronically in AD and acutely in areas affected by stroke may lead to accumulation of plasma proteins along the vessel walls that serves as a physical impediment for clearance along these spaces.

Our data support the possibility of a direct interaction between cerebrovascular pathology, ISF flow, and Aβ deposition. Epidemiological studies have demonstrated a strong association between vascular factors predisposing to cerebrovascular disease, stroke and AD [17,23,26,30] and population based neuropathological studies have shown that mixed Alzheimer's and vascular ischemic pathologies are the major correlates of dementia in the elderly, suggesting that a link may exist between the two cerebral lesions [28,46]. We have recently shown that focal stroke can trigger accelerated amyloid deposition in mouse models

of AD [13]. Aβ is present in the ISF [8] and its deposits have been observed post mortem in perivascular spaces of human AD patients [40]. Moreover, the accumulation of Aβ within the basement membrane of cortical capillaries and arteries is very similar to that of tracers injected into either brain parenchyma [16,45,49] or CSF [19]. The current findings suggest that impaired ISF drainage along perivascular spaces may be the mechanism for the observed enhancement of amyloid deposition following focal stroke [13]. Consistent with our findings, cerebral hypoperfusion in a CAA mouse model has recently been shown to lead to accelerated accumulation of Aβ on leptomeningeal vessels [30].

In addition to providing a mechanism by which vascular occlusion might impede ISF clearance, the current data also point to amyloid deposition itself as a factor in perivascular drainage. As ISF clearance along perivascular spaces represents one of the routes for Aβ elimination from the brain, the expected consequence of impaired ISF drainage would be increased Aβ concentration and enhanced deposition. The observed amyloid-dependent reduction in ISF drainage might thus generate a feed-forward process by which amyloid deposition promotes more amyloid deposition. A range of structural and functional alterations in the cerebrovasculature have been reported in the aging human and mouse brain [5,16,22,41]. CAA in particular has been associated with loss of smooth muscle cells, thickening of the basement membrane, narrowing of the vessel lumen, loss of cerebrovascular autoregulation, decreased vascular reactivity and increased occurrence of microscopic infarcts [35,37,38,41,42], all of which may further delay ISF drainage and thus exacerbate the progression of amyloid pathology. As discussed previously, focal ischemic insult impairs ISF drainage which in turn leads to increased Aβ deposition in the parenchyma and on vessel walls. Conversely, severe CAA is associated with increased occurrence of microinfarcts [38] which may further delay ISF drainage and contribute to the build-up of Aβ as well as to cognitive decline. Unlike acute focal stroke, the changes in vessel physiology during the development of CAA are progressing over a long period of time, leading to hypoperfusion and loss of cerebrovascular autoregulation, which gradually contribute to the development of the ischemic process which further exacerbates ISF drainage and the pathology in the affected areas.

Our findings are consistent with a recent report of impairments in ISF drainage in aged brains that was further aggravated in aged Tg2576 mice [16]. ISF drainage was quantified as the number of dextran positive vessels in the brain counted post mortem and showed a lower number of dextran positive capillaries in aged Tg2576 mice, in agreement with a decreased density of capillaries in the hippocampus in the same animals. Increased numbers of dextran positive veins were also observed in the old Tg2576 mice. Our use of real-time imaging of ISF drainage for individual vessel segments has the advantage of eliminating the potential confound of variations in vessel density introduced with the postmortem approach. We also note that unlike the prior study, we did not observe dextran clearance along veins, suggesting that perivascular clearance occurs only in arteries and capillaries, which are also the vessels affected by CAA. Notably, since we used a double transgenic mouse model with accelerated amyloid deposition, our animals could be studied at 6–8 months of age, a range where vascular aging per se is minimal.

In summary, the novel method of real-time imaging described here offers insights into both the mechanisms that control solute homeostasis in the living brain and into potentially important determinants of amyloid clearance and deposition. Our findings strengthen the notion of bulk flow as the primary method for ISF clearance and suggest a major role for intravascular blood flow in driving this process. These data also link cerebrovascular risk factors to impaired ISF clearance leading to dyshomeostasis of solutes in the brain that could underlie a range of neurological disorders. Our data support a feed-forward mechanism by

which CAA-related impairments in vascular function may continually promote and accelerate further Aβ deposition.

Acknowledgments

We wish to express our gratitude to Dr. K.V Kuchibhotla, Dr. A. Serrano-Pozo and Dr. T.L Spires-Jones for fruitful discussions and careful reading and editing of the manuscript. This work was supported by the National Institute of Health (grant number EB000768).

References

1. Abbott NJ. Evidence for bulk flow of brain interstitial fluid: significance for physiology and pathology. Neurochemistry international. 2004; 45:545–552.10.1016/j.neuint.2003.11.006 [PubMed: 15186921]
2. Attems J, Jellinger KA, Lintner F. Alzheimer's disease pathology influences severity and topographical distribution of cerebral amyloid angiopathy. Acta neuropathologica. 2005; 110:222–231.10.1007/s00401-005-1064-y [PubMed: 16133541]
3. Bell RD, Sagare AP, Friedman AE, Bedi GS, Holtzman DM, Deane R, Zlokovic BV. Transport pathways for clearance of human Alzheimer's amyloid beta-peptide and apolipoproteins E and J in the mouse central nervous system. Journal of cerebral blood flow and metabolism: official journal of the International Society of Cerebral Blood Flow and Metabolism. 2007; 27:909–918.10.1038/sj.jcbfm.9600419 [PubMed: 17077814]
4. Bradbury MW, Cserr HF, Westrop RJ. Drainage of cerebral interstitial fluid into deep cervical lymph of the rabbit. The American journal of physiology. 1981; 240:F329–336. [PubMed: 7223890]
5. Burns EM, Kruckeberg TW, Gaetano PK. Changes with age in cerebral capillary morphology. Neurobiology of aging. 1981; 2:283–291. [PubMed: 7335147]
6. Carare RO, Bernardes-Silva M, Newman TA, Page AM, Nicoll JA, Perry VH, Weller RO. Solutes, but not cells, drain from the brain parenchyma along basement membranes of capillaries and arteries: significance for cerebral amyloid angiopathy and neuroimmunology. Neuropathology and applied neurobiology. 2008; 34:131–144.10.1111/j.1365-2990.2007.00926.x [PubMed: 18208483]
7. Casley-Smith JR, Foldi-Borsok E, Foldi M. The prelymphatic pathways of the brain as revealed by cervical lymphatic obstruction and the passage of particles. British journal of experimental pathology. 1976; 57:179–188. [PubMed: 773400]
8. Cirrito JR, May PC, O'Dell MA, Taylor JW, Parsadanian M, Cramer JW, Audia JE, Nissen JS, Bales KR, Paul SM, DeMattos RB, Holtzman DM. In vivo assessment of brain interstitial fluid with microdialysis reveals plaque-associated changes in amyloid-beta metabolism and half-life. The Journal of neuroscience: the official journal of the Society for Neuroscience. 2003; 23:8844–8853. [PubMed: 14523085]
9. Datta S, Satten E. Rank-Sum Tests for Clustered Data. J Am Stat Assoc. 2005; 100:908–915.10.1198/016214504000001583
10. DeMattos RB, Bales KR, Cummins DJ, Paul SM, Holtzman DM. Brain to plasma amyloid-beta efflux: a measure of brain amyloid burden in a mouse model of Alzheimer's disease. Science. 2002; 295:2264–2267.10.1126/science.1067568 [PubMed: 11910111]
11. Dietrich WD, Prado R, Halley M, Watson BD. Microvascular and neuronal consequences of common carotid artery thrombosis and platelet embolization in rats. Journal of neuropathology and experimental neurology. 1993; 52:351–360. [PubMed: 8355024]
12. Fiala M, Lin J, Ringman J, Kermani-Arab V, Tsao G, Patel A, Lossinsky AS, Graves MC, Gustavson A, Sayre J, Sofroni E, Suarez T, Chiappelli F, Bernard G. Ineffective phagocytosis of amyloid-beta by macrophages of Alzheimer's disease patients. Journal of Alzheimer's disease: JAD. 2005; 7:221–232. discussion 255–262.
13. Garcia-Alloza M, Gregory J, Kuchibhotla KV, Fine S, Wei Y, Ayata C, Frosch MP, Greenberg SM, Bacskai BJ. Cerebrovascular lesions induce transient beta-amyloid deposition. Brain: a journal of neurology. 2011; 134:3697–3707.10.1093/brain/awr300 [PubMed: 22120142]

14. Garcia-Alloza M, Robbins EM, Zhang-Nunes SX, Purcell SM, Betensky RA, Raju S, Prada C, Greenberg SM, Bacskai BJ, Frosch MP. Characterization of amyloid deposition in the APPswe/PS1dE9 mouse model of Alzheimer disease. Neurobiology of disease. 2006; 24:516–524.10.1016/j.nbd.2006.08.017 [PubMed: 17029828]
15. Greenberg SM, Gurol ME, Rosand J, Smith EE. Amyloid angiopathy-related vascular cognitive impairment. Stroke; a journal of cerebral circulation. 2004; 35:2616–2619.10.1161/01.STR.0000143224.36527.44
16. Hawkes CA, Hartig W, Kacza J, Schliebs R, Weller RO, Nicoll JA, Carare RO. Perivascular drainage of solutes is impaired in the ageing mouse brain and in the presence of cerebral amyloid angiopathy. Acta neuropathologica. 2011; 121:431–443.10.1007/s00401-011-0801-7 [PubMed: 21259015]
17. Helzner EP, Luchsinger JA, Scarmeas N, Cosentino S, Brickman AM, Glymour MM, Stern Y. Contribution of vascular risk factors to the progression in Alzheimer disease. Archives of neurology. 2009; 66:343–348.10.1001/archneur.66.3.343 [PubMed: 19273753]
18. Hrabetova, S.; Nicholson, C. Biophysical Properties of Brain Extracellular Space Explored with Ion-Selective Microelectrodes, Integrative Optical Imaging and Related Techniques. In: Michael, AC.; Borland, LM., editors. Electrochemical Methods for Neuroscience, City. 2007.
19. Iliff JJ, Wang M, Liao Y, Plogg BA, Peng W, Gundersen GA, Benveniste H, Vates GE, Deane R, Goldman SA, Nagelhus EA, Nedergaard M. A paravascular pathway facilitates CSF flow through the brain parenchyma and the clearance of interstitial solutes, including amyloid beta. Science translational medicine. 2012; 4:147ra111.10.1126/scitranslmed.3003748
20. Iwata N, Higuchi M, Saido TC. Metabolism of amyloid-beta peptide and Alzheimer's disease. Pharmacology & therapeutics. 2005; 108:129–148.10.1016/j.pharmthera.2005.03.010 [PubMed: 16112736]
21. Jankowsky JL, Slunt HH, Ratovitski T, Jenkins NA, Copeland NG, Borchelt DR. Co-expression of multiple transgenes in mouse CNS: a comparison of strategies. Biomolecular engineering. 2001; 17:157–165. [PubMed: 11337275]
22. Kalaria RN. Cerebral vessels in ageing and Alzheimer's disease. Pharmacology & therapeutics. 1996; 72:193–214. [PubMed: 9364575]
23. Kalaria RN. The role of cerebral ischemia in Alzheimer's disease. Neurobiology of aging. 2000; 21:321–330. [PubMed: 10867217]
24. Kleinfeld D, Mitra PP, Helmchen F, Denk W. Fluctuations and stimulus-induced changes in blood flow observed in individual capillaries in layers 2 through 4 of rat neocortex. Proceedings of the National Academy of Sciences of the United States of America. 1998; 95:15741–15746. [PubMed: 9861040]
25. Klunk WE, Bacskai BJ, Mathis CA, Kajdasz ST, McLellan ME, Frosch MP, Debnath ML, Holt DP, Wang Y, Hyman BT. Imaging Abeta plaques in living transgenic mice with multiphoton microscopy and methoxy-X04, a systemically administered Congo red derivative. Journal of neuropathology and experimental neurology. 2002; 61:797–805. [PubMed: 12230326]
26. Launer LJ, Petrovitch H, Ross GW, Markesbery W, White LR. AD brain pathology: vascular origins? Results from the HAAS autopsy study. Neurobiology of aging. 2008; 29:1587–1590.10.1016/j.neurobiolaging.2007.03.008 [PubMed: 17466414]
27. Morrison PF, Laske DW, Bobo H, Oldfield EH, Dedrick RL. High-flow microinfusion: tissue penetration and pharmacodynamics. The American journal of physiology. 1994; 266:R292–305. [PubMed: 8304553]
28. Aging S. Neuropathology Group. Medical Research Council Cognitive F. Pathological correlates of late-onset dementia in a multicentre, community-based population in England and Wales. Neuropathology Group of the Medical Research Council Cognitive Function and Ageing Study (MRC CFAS). Lancet. 2001; 357:169–175. [PubMed: 11213093]
29. Nicholson C. Diffusion from an injected volume of a substance in brain tissue with arbitrary volume fraction and tortuosity. Brain research. 1985; 333:325–329. [PubMed: 3995298]
30. Okamoto Y, Yamamoto T, Kalaria RN, Senzaki H, Maki T, Hase Y, Kitamura A, Washida K, Yamada M, Ito H, Tomimoto H, Takahashi R, Ihara M. Cerebral hypoperfusion accelerates

cerebral amyloid angiopathy and promotes cortical microinfarcts. Acta neuropathologica. 2012; 123:381–394.10.1007/s00401-011-0925-9 [PubMed: 22170742]

31. Paulson OB, Waldemar G, Schmidt JF, Strandgaard S. Cerebral circulation under normal and pathologic conditions. The American journal of cardiology. 1989; 63:2C–5C.
32. Robbins EM, Betensky RA, Domnitz SB, Purcell SM, Garcia-Alloza M, Greenberg C, Rebeck GW, Hyman BT, Greenberg SM, Frosch MP, Bacskai BJ. Kinetics of cerebral amyloid angiopathy progression in a transgenic mouse model of Alzheimer disease. The Journal of neuroscience: the official journal of the Society for Neuroscience. 2006; 26:365–371.10.1523/JNEUROSCI.3854-05.2006 [PubMed: 16407531]
33. Shibata M, Yamada S, Kumar SR, Calero M, Bading J, Frangione B, Holtzman DM, Miller CA, Strickland DK, Ghiso J, Zlokovic BV. Clearance of Alzheimer's amyloid-ss(1–40) peptide from brain by LDL receptor-related protein-1 at the blood-brain barrier. The Journal of clinical investigation. 2000; 106:1489–1499.10.1172/JCI10498 [PubMed: 11120756]
34. Shih AY, Blinder P, Tsai PS, Friedman B, Stanley G, Lyden PD, Kleinfeld D. The smallest stroke: occlusion of one penetrating vessel leads to infarction and a cognitive deficit. Nature neuroscience. 2013; 16:55–63.10.1038/nn.3278
35. Shin HK, Jones PB, Garcia-Alloza M, Borrelli L, Greenberg SM, Bacskai BJ, Frosch MP, Hyman BT, Moskowitz MA, Ayata C. Age-dependent cerebrovascular dysfunction in a transgenic mouse model of cerebral amyloid angiopathy. Brain: a journal of neurology. 2007; 130:2310–2319.10.1093/brain/awm156 [PubMed: 17638859]
36. Skoch J, Hickey GA, Kajdasz ST, Hyman BT, Bacskai BJ. In vivo imaging of amyloid-beta deposits in mouse brain with multiphoton microscopy. Methods in molecular biology. 2005; 299:349–363. [PubMed: 15980616]
37. Smith EE, Vijayappa M, Lima F, Delgado P, Wendell L, Rosand J, Greenberg SM. Impaired visual evoked flow velocity response in cerebral amyloid angiopathy. Neurology. 2008; 71:1424–1430.10.1212/01.wnl.0000327887.64299.a4 [PubMed: 18955685]
38. Soontornniyomkij V, Lynch MD, Mermash S, Pomakian J, Badkoobehi H, Clare R, Vinters HV. Cerebral microinfarcts associated with severe cerebral beta-amyloid angiopathy. Brain pathology. 2010; 20:459–467.10.1111/j.1750-3639.2009.00322.x [PubMed: 19725828]
39. Szentistvanyi I, Patlak CS, Ellis RA, Cserr HF. Drainage of interstitial fluid from different regions of rat brain. The American journal of physiology. 1984; 246:F835–844. [PubMed: 6742132]
40. Utter S, Tamboli IY, Walter J, Upadhaya AR, Birkenmeier G, Pietrzik CU, Ghebremedhin E, Thal DR. Cerebral small vessel disease-induced apolipoprotein E leakage is associated with Alzheimer disease and the accumulation of amyloid beta-protein in perivascular astrocytes. Journal of neuropathology and experimental neurology. 2008; 67:842–856.10.1097/NEN.0b013e3181836a71 [PubMed: 18716559]
41. Vinters HV. Cerebral amyloid angiopathy. A critical review. Stroke; a journal of cerebral circulation. 1987; 18:311–324.
42. Viswanathan A, Greenberg SM. Cerebral amyloid angiopathy in the elderly. Annals of neurology. 2011; 70:871–880.10.1002/ana.22516 [PubMed: 22190361]
43. Watson BD, Dietrich WD, Busto R, Wachtel MS, Ginsberg MD. Induction of reproducible brain infarction by photochemically initiated thrombosis. Annals of neurology. 1985; 17:497–504.10.1002/ana.410170513 [PubMed: 4004172]
44. Weed LH. Studies on Cerebro-Spinal Fluid. No. III: The pathways of escape from the Subarachnoid Spaces with particular reference to the Arachnoid Villi. The Journal of medical research. 1914; 31:51–91. [PubMed: 19972194]
45. Weller RO, Massey A, Newman TA, Hutchings M, Kuo YM, Roher AE. Cerebral amyloid angiopathy: amyloid beta accumulates in putative interstitial fluid drainage pathways in Alzheimer's disease. The American journal of pathology. 1998; 153:725–733. [PubMed: 9736023]
46. Wilson RS, Scherr PA, Schneider JA, Tang Y, Bennett DA. Relation of cognitive activity to risk of developing Alzheimer disease. Neurology. 2007; 69:1911–1920.10.1212/01.wnl.0000271087.67782.cb [PubMed: 17596582]

47. Wisniewski HM, Kozlowski PB. Evidence for blood-brain barrier changes in senile dementia of the Alzheimer type (SDAT). Annals of the New York Academy of Sciences. 1982; 396:119–129. [PubMed: 6185032]

48. Woollam DH, Millen JW. The perivascular spaces of the mammalian central nervous system and their relation to the perineuronal and subarachnoid spaces. Journal of anatomy. 1955; 89:193–200. [PubMed: 14367214]

49. Yamaguchi H, Yamazaki T, Lemere CA, Frosch MP, Selkoe DJ. Beta amyloid is focally deposited within the outer basement membrane in the amyloid angiopathy of Alzheimer's disease. An immunoelectron microscopic study. The American journal of pathology. 1992; 141:249–259. [PubMed: 1632466]

50. Zhang ET, Richards HK, Kida S, Weller RO. Directional and compartmentalised drainage of interstitial fluid and cerebrospinal fluid from the rat brain. Acta neuropathologica. 1992; 83:233–239. [PubMed: 1373020]

51. Zhang S, Murphy TH. Imaging the impact of cortical microcirculation on synaptic structure and sensory-evoked hemodynamic responses in vivo. PLoS biology. 2007; 5:e119.10.1371/journal.pbio.0050119 [PubMed: 17456007]

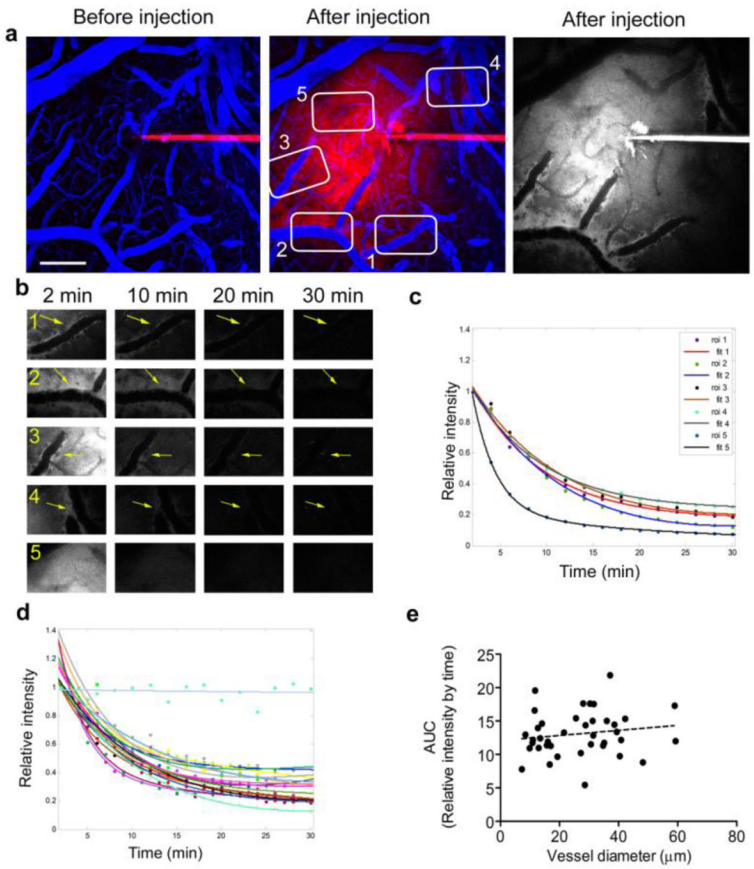

Fig. 1. Characterization of ISF drainage in the healthy mouse brain

To visualize ISF drainage in the mouse cortex, a 3kDa dextran conjugated to Cascade Blue was injected into the brain parenchyma at about 150μm depth via a thin glass pipette. A 70kDa dextran conjugated to Texas-Red was injected i.v for visualization of the brain vasculature. (a) Images represent the merged maximal projections of cortical volumes before and after the dextran injection (Texas Red in blue and Cascade Blue in red). A single channel maximal projection is shown in grey to better visualize the Cascade Blue alignment along vessel walls. The numbered white boxes indicate regions of interest (ROI) selected for quantification showed in (b). Dye alignment along vessel walls (ROI 1–4, yellow arrows) and its presence in the parenchyma (ROI 5) were followed for 30 min and quantified. (c) Dye intensity in the selected ROIs normalized to the intensity measured in the first time point (2 min post injection), shows a bi-exponential mode of decay. (d) Dye clearance along vessels from healthy brains (15 vessels from 6 different brains) shows a uniform pattern with low variability. Imaging Cascade Blue in the glass pipette above the brain surface shows no bleaching over time (light blue linear fit). (e) Area under the curve (AUC), calculated for each vessel, shows no correlation of ISF drainage with vessel diameter (0.005 ± 0.029 mean increase/μm, p=0.861). Scale bar = 100μm.

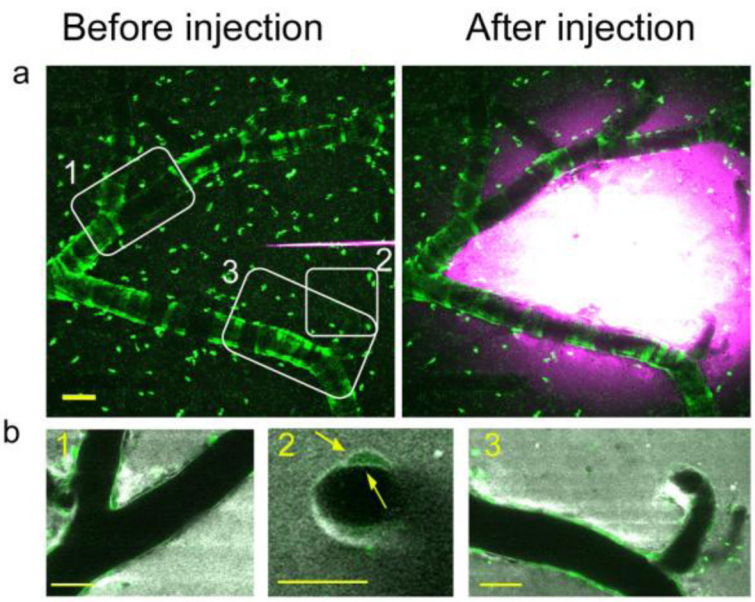

Fig. 2. Spatial distribution of dye accumulation in the brain

The localization of the dye along the vessels and within the basement membrane was investigated by performing the bolus dye injections of cascade blue dextran in mice that express EGFP in their smooth muscle cells (Myh11-cre,-EGFP mice). (a) Representative maximum intennsity projection image of cortical volumes before and soon after bolus dye injection (Individual smooth muscle cells are evident in green, cascade blue is shown in magenta). White boxes show areas that are presented in (b). Individual slices, 5μm thick, of the areas denoted in the white boxes are shown (smooth muscle cells – green, cascade blue dextran – gray). Dextran accumulation is evident along the vessel length (boxes 1 and 3) in the perivascular space and/or parenchyma as well as within the basement membrane between the smooth muscle cells, as indicated by the yellow arrows in box 2. Scale bars=50μm.

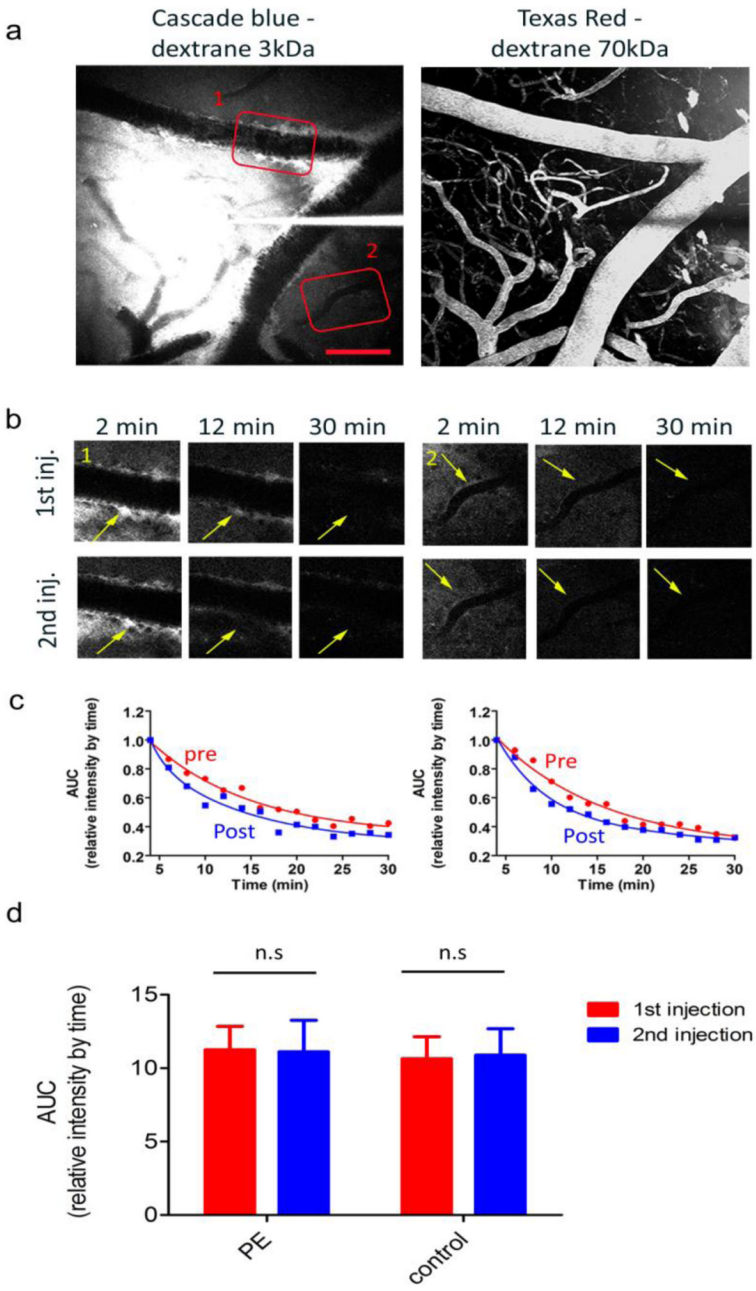

Fig. 3. Transient systemic hypertension does not affect perivascular ISF drainage

The effects of mild systemic hypertension on ISF drainage was investigated by performing two consecutive bolus dye injections, each followed by time lapse imaging and peripheral application of phenylephrine (PE), between the two injections. (a) Representative maximal projection image of cortical volumes rapidly after bolus dye injection showing the Cascade Blue Dextran (shown in red) injected in the parenchyma and the brain vasculature labeled with Texas red (shown in blue). Red boxes represent dye alignment along vessel walls that was monitored over time (b) and quantified (c) before and after peripheral injection of PE (1^{st} and 2^{nd} injections, respectively). (d). Summary of area under the curve (AUC), calculated for each vessel segment, after the 1^{st} and 2^{nd} injections in six separate PE experiments (18 vessels) and seven separate control experiments (PBS injection; 20 vessels).

Values presented represent the mean and S.E.M. Post vs. pre comparisons:PE – p=0.88; controls – p=0.705. Scale bar = 100μm.

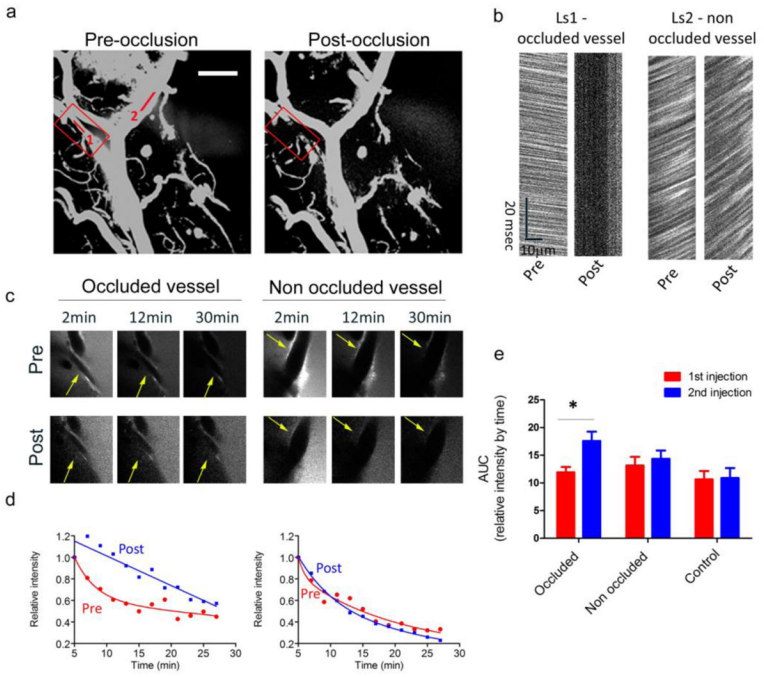

Fig. 4. Focal micro-strokes impair perivascular ISF drainage

The effects of focal stroke on ISF drainage was investigated by performing two consecutive bolus dye injections, each followed by time lapse imaging, and application of focal stroke between the two injections. (a). Maximal intensity projection images of the brain vasculature before and after the Rose Bengal-induced microstroke ('occlusion', marked by a red box). (b) Bi-directional line scans along the vessel length were used to measure RBC velocity in the occluded and a non-occluded vessel (1 and 2 shown in A, respectively). Presented LS show the cessation of blood flow in the occluded area with minimal effect in the non-occluded area (Ls1 and Ls2, respectively). (c) Representative images of dye alignments along vessels, from the time lapse imaging in the occluded and non-occluded vessels pre- and post-occlusion are shown. (d) Dye intensities in occluded vessel and non-occluded vessel were quantified and plotted after the first and second injections (pre and post, respectively), showing a dramatic impairment in the dye clearance along the occluded vessel. (e) Summary of the area under the curve (AUC) parameter, calculated for each vessel segment, before and after occlusion, in six separate stroke experiments (6 occluded vessels, 21 non occluded vessels) as well as seven separate control experiments (no application of stroke; 20 vessels). Values presented represent the mean and S.E.M calculated using a mixed effects regression model, with random effects for mouse to adjust for within-mouse correlation, * $p<0.001$. Scale bar = 100μm

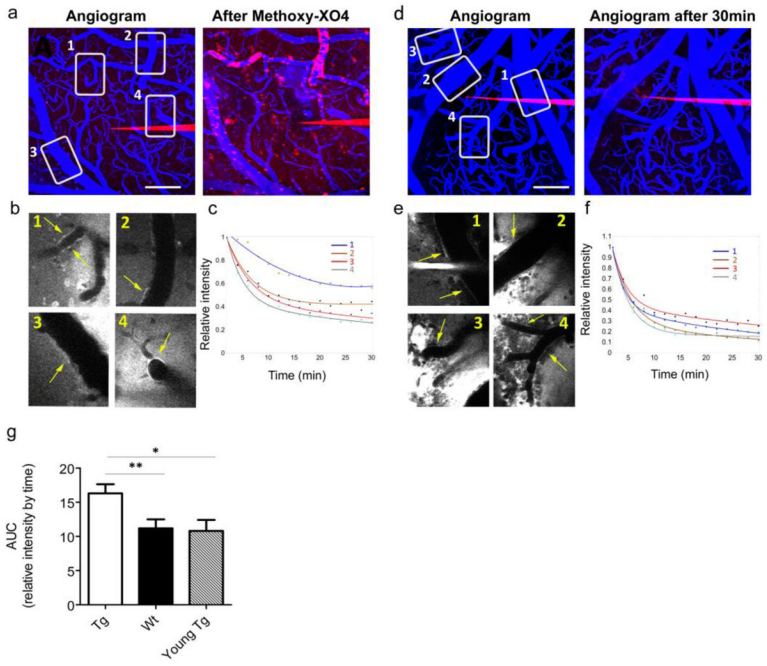

Fig. 5. ISF perivascular drainage is impaired in transgenic mice with deposited plaques and CAA

The effect of amyloid deposition on ISF drainage was investigated in APP/PS1 transgenic mice and wild type littermates. (a–c) An example for dye parenchymal injection in aged transgenic mice. (a) Maximal projections of cortical volumes before the dye injections (Cascade-Blue dextran in red, Texas-red dextran in blue) and at the end of the experiment after injection of Methoxy-XO4 which labels the amyloid pathology (Methoxy-XO4 also shown in red). Numbered boxes outline areas in which dye alignment was quantified over time. (b) Single 5μm images showing dextran alignment along vessel walls corresponding to the boxes in a (yellow arrows indicate quantified areas). (c) Dye intensity decay curves fitted with bi-exponential models. (d–f) A similar experiment performed in an age-matched wild type littermate. (d) Maximal projections before and 30 min after the dye injections are shown. Numbered boxes outline areas in which dye alignment was quantified over time. (e) Single 5μm slice showing dextran alignment along vessel walls of the boxes in d (yellow arrows indicate quantified areas). (f) Dye intensity decay curves fitted with bi-exponential models. (g) AUC summary, calculated for each vessel segment from transgenic and wild-type animals at 6–8 months of age (n=8 mice/group; tg- 24 vessels; wt −28 vessels) as well as in young pre-plaque transgenic mice at 2.5–3months of age (n=5 mice, 20 vessels). Values represent the mean and S.E.M. ** p=0.007; *p= 0.011. Scale bar = 100μm.